

Electron Spin-Echo Envelope Modulation Spectroscopy of Mn²⁺·GDP Complexes of N-ras p21 with Selective ¹⁵N Labeling

Russell G. Larsen,[§] Christopher J. Halkides,[†] Alfred G. Redfield,[†] and David J. Singel^{*§}

Contribution from the Department of Chemistry, Harvard University, Cambridge, Massachusetts 02138, and Department of Biochemistry, Brandeis University, Waltham, Massachusetts 02254. Received April 13, 1992

Abstract: A multifrequency ESEEM study of Mn²⁺·GDP complexes of N-ras p21 with selective ¹⁵N labeling is reported. Nuclear modulation effects from ³¹P at the α and β positions of GDP and ¹⁵N at serine and glycine labeled amide positions are observed. Electron-nuclear hyperfine interactions are obtained for these nuclei from an analysis of spectral frequencies and amplitudes. This analysis considers both the impact of the high electron spin multiplicity of Mn²⁺ and the influence of partial isotopic enrichment with ¹⁵N, which is assessed by GC/MS. Interpretation of the anisotropic portion of the nuclear hyperfine interaction as a classical magnetic dipole interaction enables the calculation of distances between the nuclei and Mn²⁺ that are in excellent agreement with results obtained by X-ray crystallography.

Introduction

The structure and function of p21, a guanine nucleotide binding protein of $M_r \approx 21\,000$ encoded by *ras* genes,^{1,2} are being intensively studied. Conformational changes in p21, associated with the hydrolysis of bound Mg²⁺·GTP to Mg²⁺·GDP, are thought to play a pivotal role in the transduction of signals for cellular growth and differentiation.³⁻⁵ Hydrolysis of the GTP present in growth-active p21 is normally promoted by its association with the proteins GAP or NF-1.⁶ These proteins are not effective, however, in terminating growth signals in point-mutations of p21 commonly found in many types of human cancer cells.¹ X-ray crystallographic studies of various forms of p21^{4,5} have led to the development of models for the path of GTP hydrolysis as well as the obstacles laid by oncogenic mutations.⁵ The relevance of these studies of *isolated* p21 proteins to the mechanism of GAP or NF-1 promoted GTP hydrolysis remains uncertain.

We are presently exploiting an electron-nuclear magnetic resonance method, ESEEM^{7,8} (electron spin-echo envelope modulation), to probe the chemical constitution and the structure of the GDP/GTP binding site in Mn²⁺ guanine nucleotide complexes of p21. ESEEM is a solid-state (frozen solution) magnetic resonance technique in which the magnetic nuclei in a region of the molecule near a paramagnetic probe, such as Mn²⁺, are selectively monitored through their modulation of the electron spin-echo decay. These modulations, at the nuclear spin resonance frequencies, provide a means to measure electron-nuclear hyperfine couplings, which in turn can be related to the distance between the nuclei and the probe.⁹ ESEEM does not require single crystals, nor is it restricted to protein assemblies of modest molecular weight. It is thus not only well-suited for probing structural details of p21 in solution, but also is perhaps uniquely suited for probing the impact of the binding of large proteins such as GAP and NF-1 ($M_r \approx 10^5$) on the GTPase site of p21.

A crucial first stage in this investigation is to critically compare structural details obtained through ESEEM with those obtained by crystallography. This comparison verifies the simple picture that we employ in the analysis of Mn²⁺ ESEEM data, the adequacy of the classical dipole model for relating hyperfine couplings to interatomic distances, and the structural innocence of Mn²⁺ substitution for Mg²⁺ in p21 complexes. Consistent with these aims we focus, in the fundamental experiments detailed here, on examining the structurally well-defined nucleotide binding domains of the GDP complex of p21; we report the observation and analysis of ESEEM from ³¹P of the GDP, and from ¹⁵N incorporated at

amide positions in serine and glycine residues in the Mn²⁺·GDP complex of p21.

Experimental Methods

Isotopically labeled proteins were prepared as described previously,^{10,11} except that the plasmids carried the human N-ras p21 gene behind the *tac* promoter. The protein was refolded in the presence of GDP and Mg²⁺ from an insoluble fraction, then purified by anion-exchange chromatography.¹² The isotopic enrichment of the amino acid residues was

(1) Barbacid, M. *Annu. Rev. Biochem.* **1987**, *56*, 779-827.

(2) Grand, J. A.; Owen, D. *Biochem. J.* **1991**, *279*, 609-631.

(3) (a) Bourne, H. R.; Sanders, D. A.; McCormick, F. *Nature* **1990**, *348*, 125-132. (b) Bourne, H. R.; Sanders, D. A.; McCormick, F. *Nature* **1991**, *349*, 117-126.

(4) (a) Kregel, U.; Schlichting, I.; Scherer, A.; Schumann, R.; Frech, M.; John, J.; Kabsch, W.; Pai, E. F.; Wittinghofer, A. *Cell* **1990**, *62*, 539-548. (b) Pai, E. F.; Kregel, U.; Petsko, G. A.; Goody, R. S.; Kabsch, W.; Wittinghofer, A. *EMBO J.* **1990**, *9*, 2351-2359. (c) Pai, E. F.; Kabsch, W.; Kregel, W.; Holmes, K. C.; John, J.; Wittinghofer, A. *Nature* **1989**, *341*, 209-214. (d) Schlichting, I.; Almo, S. C.; Rapp, G.; Wilson, K.; Petrats, K.; Lentfer, A.; Wittinghofer, A.; Kabash, W.; Pai, E.; Petsko, G. A.; Goody, R. S. *Nature* **1990**, *345*, 309-315. (e) Schlichting, I.; Rapp, G.; John, J.; Wittinghofer, A.; Pai, E.; Goody, R. S. *Proc. Natl. Acad. Sci. U.S.A.* **1989**, *86*, 7687-7690. (f) Saraste, M.; Sibbald, P. R.; Wittinghofer, A. *TIBS* **1990**, *15*, 430-434.

(5) (a) Tong, L.; DeVos, A. M.; Milburn, M. V.; Jancarik, J.; Noguchi, S.; Nishimura, S.; Miura, K.; Ohtsuka, E.; Kim, S. *Nature* **1989**, *337*, 90-93. (b) DeVos, A. M.; Tong, L.; Milburn, M. V.; Matias, P. M.; Jancarik, J.; Noguchi, S.; Nishimura, S.; Miura, K.; Ohtsuka, E.; Kim, S. *Science* **1988**, *239*, 888-893. (c) Tong, L.; Milburn, M. V.; De Vos, A. M.; Kim, S. *Science* **1989**, *239*, 244. (d) Milburn, M. V.; Tong, L.; DeVos, A. M.; Brunger, A.; Yamaizumi, Z.; Nishimura, S.; Kim, S. *Science* **1990**, *247*, 939-945.

(6) Martin, G. A.; Viskochil, D.; Bollag, G.; McCabe, P. C.; Crosier, W. J.; Haubruck, H.; Conroy, L.; Clark, R.; O'Connell, P.; Cawthon, R. M.; Innis, M. A.; McCormick, F. *Cell* **1990**, *63*, 843-849.

(7) (a) Rowan, L. G.; Hahn, E. L.; Mims, W. B. *Phys. Rev.* **1965**, *137*, 61-71. (b) Mims, W. B. *Phys. Rev.* **1972**, *B5*, 2409-2418. (c) Mims, W. B. *Phys. Rev.* **1972**, *6*, 3543-3546.

(8) (a) Mims, W. B.; Peisach, J. *Biological Magnetic Resonance*; Berliner, L. J., Reuben, J., Eds.; Plenum: New York, 1981; Vol. 3, pp 213-263. (b) Thomann, H.; Dalton, L. R.; Dalton, L. A. *Biological Magnetic Resonance*; Berliner, L. J., Reuben, J., Eds.; Plenum: New York, 1984; Vol. 6, pp 143-186. (c) Tsevtkov, Y. D.; Dikanov, S. A. *Metal Ions in Biological System*; Sigel, H., Ed.; Marcel Dekker: New York, 1987; Vol. 22, pp 207-263.

(9) To a good approximation, the anisotropic hyperfine interaction can be treated, for nuclei not directly coordinated to the Mn²⁺, as a classical magnetic dipole interaction between magnetic dipoles located at the nuclear and electronic Mn²⁺ positions: (a) Metz, H., et al. *Chem. Phys. Lett.* **1982**, *89*, 351. (b) DeBeer, R.; DeBoer, C. A.; Van't Hof, C. A.; Van Ormondt, D. *Acta Crystallogr., Sect. B* **1973**, *B29*, 1473-1480. (c) Van Ormondt, D.; DeBeer, R.; Brouha, M.; De Groot, F. Z. *Naturforsch.* **1969**, *24a*, 1746-1751.

(10) LeMaster, D. M.; Richards, F. M. *Biochemistry* **1988**, *27*, 142-150.

(11) Redfield, A. G.; Papastavros, M. Z. *Biochemistry* **1990**, *29*, 3509-3514.

[§] Harvard University.

[†] Brandeis University.

* Author to whom correspondence should be addressed at: Department of Chemistry, Harvard University, 12 Oxford St., Cambridge, MA 02138.

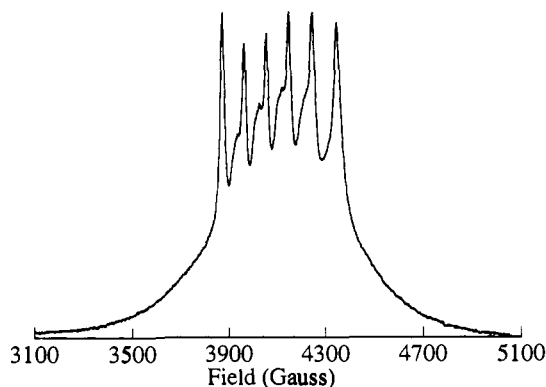


Figure 1. Echo-detected EPR (11.68 GHz, 4.2 K) of a Mn^{2+} -GDP complex of p21.

determined by GC/MS of derivatives (Alltech) of the amino acids that were obtained by complete hydrolysis of the protein.¹³

Samples of protein were converted into the manganese form by dialysis against buffer containing 1–5 mM $MnCl_2$ and 1 μM GDP, followed by dialysis against buffer containing 1 μM $MnCl_2$ and GDP. This procedure leads to stoichiometric incorporation of Mn^{2+} in p21, with no significant trace of unbound Mn^{2+} as assessed by EPR spectroscopy. For ESEEM experiments, which were conducted at 4.2 K, an aliquot (ca. 50% by volume) of glycerol was added to the samples to inhibit solvent crystallization during freezing. The samples used for ESEEM were ~ 0.15 mL in volume with a p21 concentration of ~ 0.5 mM.

Two- and three-pulse ESEEM experiments were carried out in a spectrometer described previously.¹⁴ The ESEEM patterns recorded typically consist of three scans of 200 time-domain steps of 10–15 ns. At each step ~ 500 electron spin-echoes were accumulated, at a repetition rate of ~ 300 Hz. ESEEM patterns were recorded at microwave frequencies in the range of 8–12 GHz. Typically the ESEEM spectra were obtained with excitation at EPR intensity maxima. For any given sample, ESEEM observations were made at no fewer than 18 distinct resonant fields and frequencies.

Spectral analysis of the ESEEM patterns was performed in the following manner. To minimize the spectral amplitude in the zero-frequency neighborhood, which is dominated by the overall echo decay rather than by nuclear modulation effects, a decay function was fitted to the time-domain pattern and subtracted from it. We employed LP-SVD routines, as described previously,¹⁴ or linear least-squares fitting routines to determine Gaussian, exponential, or fifth-order polynomial decay profiles. Spectral analysis of the calculated decay functions revealed no significant amplitude beyond 1 MHz. The residual pattern was then multiplied by an extended cosine bell window function, zero-filled, and Fourier transformed.

We employ numerical simulations of the ESEEM spectra to evaluate the relevant nuclear hyperfine coupling constants. The simulation begins with a calculation of the ESEEM frequencies and amplitudes, according to the theory of Mims,⁷ which we have elaborated, as summarized in the Appendix to this article, to account for the effects of high electron spin multiplicity. From these data we construct an ESEEM-amplitude weighted frequency histogram.¹⁴ In order to generate a spectrum that is suitable for *direct* comparison to the experimental spectrum, we inverse Fourier transform this frequency histogram, multiply the resulting time domain pattern by the decay function fitted to the relevant ESEEM data, and truncate the pattern so that it conforms to the experimental observation interval. Finally the simulated pattern, like the experimental one, is normalized to unity at its maximum, a scaling practice acceptable for weakly modulated ESE envelopes. The resulting simulated pattern is then subjected to the same battery of preprocessing and transformation methods as applied to the experimental ESEEM patterns.

This frequency-domain method of analysis has two main advantages over other approaches for the quantitative analysis of ESEEM data. In contrast to analyses of time-domain patterns, our method facilitates the isolation of specific frequency components for individual examination. Moreover, inasmuch as the simulated and experimental data are treated in identical manners, the possibility of confusion between authentic sig-

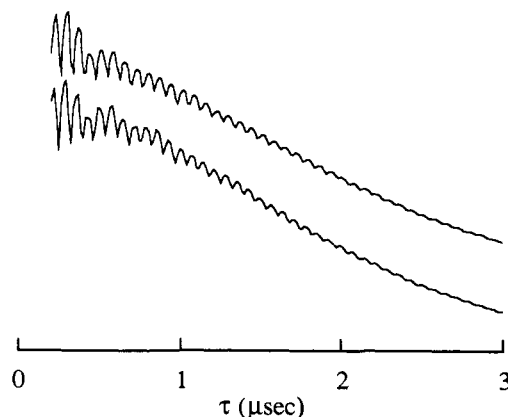


Figure 2. Two-pulse ESEEM patterns of Mn^{2+} -GDP complexes of p21 containing (top) ^{15}N amide labeled glycine (73%) and (bottom) ^{15}N amide labeled serine (40%). The patterns were recorded as described in the text at a field settings of 3274 G and excitation frequencies of 9.867 and 8.500 GHz, respectively.

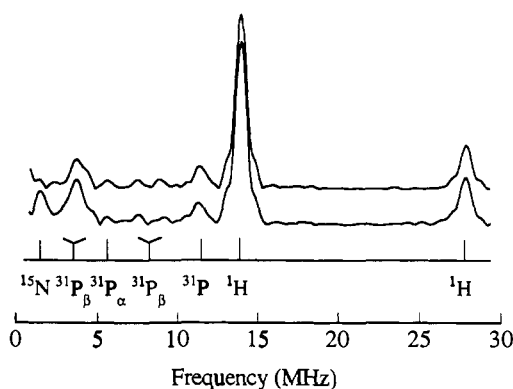


Figure 3. Two-pulse ESEEM spectra obtained, as described in the text, from the time domain patterns shown in Figure 2, of Mn^{2+} -GDP complexes of p21 containing (top) ^{15}N amide labeled glycine (73%) and (bottom) ^{15}N amide labeled serine (40%).

nals and processing artifacts is very remote. Our observation of ESEEM spectra at numerous distinct field/frequency settings provides an additional, stringent test of the significance of the features observed in the ESEEM spectra.

Results and Discussion

In Figure 1, we show an echo-detected EPR spectrum of a Mn^{2+} -GDP complex of p21. The derivative of this spectrum is essentially superimposable on the conventional CW EPR spectrum of this sample. The estimate of the zero-field splitting parameter, $D \approx 310$ MHz, made by Reed and co-workers based on simulation of CW Q-band EPR spectra,¹⁵ is consistent with the appearance of the EPR spectrum shown in the figure. The sharp central spectral features stem primarily from the $M_s = +1/2 \leftrightarrow -1/2$ transition which is split into six components by the ^{55}Mn hyperfine interaction.¹⁶ The broad background and the wings, features often artificially suppressed in CW EPR spectra, derive from the other $\Delta M_s = \pm 1$ transitions of the spin $S = 5/2$ Mn^{2+} ion. These transitions can play an important role in determining the appearance of Mn^{2+} ESEEM spectra.

In Figures 2 and 3, we show a pair of ESEEM patterns and associated spectra of the same complex of p21. These ESEEM patterns (Figure 2) were recorded at ~ 9 GHz with excitation at EPR intensity maxima. In both spectra (Figure 3), fundamental peaks are apparent at the ^{31}P and 1H Larmor frequencies (5.7 and 14.0 MHz); combination peaks appear at twice the Larmor

(12) Papastavros, M. Z.; Redfield, A. G. Unpublished results.

(13) MacKenzie, S. L. *Gas Chromatography Mass Spectrometry Applications in Microbiology*; Odham, G., Larsson, L., Mårdh, P.-A., Eds.; Plenum Press: New York, 1984; pp 161–172.

(14) Gerfen, G. J. The Magnetic Field Dependence of Electron Spin Echo Envelope Modulation. Ph.D. Thesis, Harvard University, 1990.

(15) Smithers, G. W.; Poe, M.; Latwesen, D. G.; Reed, G. H. *Arch. Biochem. Biophys.* 1990, 280, 416–420.

(16) Reed, G. H.; Markham, G. D. *Biological Magnetic Resonance*; Berliner, L. J., Reuben, J., Eds.; Plenum: New York, 1984; Vol. 6, pp 73–138.

frequencies (11.4 and 28.0 MHz). A strong peak at ~ 4 MHz and a bilobal remnant¹⁷ of a broad, weak peak at ~ 8 MHz are also evident. In the spectrum of the serine ¹⁵N-labeled sample (Figure 3, bottom), an additional peak at the ¹⁵N Larmor frequency (1.4 MHz) appears; this peak is scarcely observable in the spectrum of the sample labeled at the glycine amide position (Figure 3, top).

ESEEM has previously been employed to probe ligation at the active site in Mn²⁺ complexes of several phosphoryl group transfer enzymes.¹⁸ The influence of the high electron spin multiplicity of the electron spin $S = 5/2$ Mn²⁺ on ESEEM spectra, however, has essentially been ignored in these prior studies. We address this issue more fully elsewhere,¹⁹ but introduce the salient details of our analysis as an Appendix to this article. The various features in the ESEEM spectra of Mn²⁺ p21 complexes can be readily understood and quantitatively analyzed within the framework outlined in this Appendix.

The strong peak at ~ 4 MHz and weak peak at ~ 8 MHz derive from ³¹P of the bound, β -phosphate group of GDP, as does most of the intensity of the phosphorus combination peak at ~ 11 MHz. The intensity imbalance between the fundamental peaks reflects the influence of the high spin multiplicity of Mn²⁺ on the ESEEM spectra. Since the ³¹P hyperfine and Zeeman interactions are approximately "matched"²⁰ in the $M_s = 3/2$ level,²¹ the 4-MHz peak gains an extra measure of intensity from the $M_s = 3/2 \leftrightarrow 1/2$ EPR transition. From multifrequency ESEEM spectra obtained at 8–12 GHz, we determine the isotropic coupling constant, $A_0^0 = 4.70 \pm 0.09$ MHz and the anisotropic coupling constant, $A_2^0 = 0.86 \pm 0.04$ MHz. From this value of A_2^0 we calculate a distance of 3.3 ± 0.1 Å, in good agreement with the value of 3.6 Å found by X-ray crystallography.²²

For the weakly coupled nuclei, that is, nuclei with ESEEM frequencies indistinguishable from their free Larmor frequencies, the ESEEM amplitudes scarcely vary with M_s ; the high spin multiplicity of Mn²⁺ thus has little impact on the amplitude of Larmor frequency ESEEM. The theory previously developed to interpret modulation depths of nuclei weakly coupled to an electron spin $1/2$ is thus also applicable for coupling to Mn²⁺.²³ For a given isotopic label, the total ESEEM amplitude at ν_n is simply the sum of the contributions from all the labeled sites, with each contribution weighted by the isotopic enrichment and the square of electron-nuclear dipolar coupling, or inverse sixth power of the electron-nuclear distance.²³

Because of the severity of the distance weighting, a single closest nucleus can dominate the ESEEM spectrum of a sparsely labeled protein. The p21-GDP crystal structure²² indicates that, in the case of the serine labeled protein, the serine 17 label lies singularly close to the Mn²⁺ probe. The observed ¹⁵N peak in the lower trace of Figure 3 can thus be assigned as deriving exclusively from this amide nitrogen. To measure ¹⁵N hyperfine couplings, we analyzed the amplitude of the ¹⁵N peak observed in three-pulse ESEEM

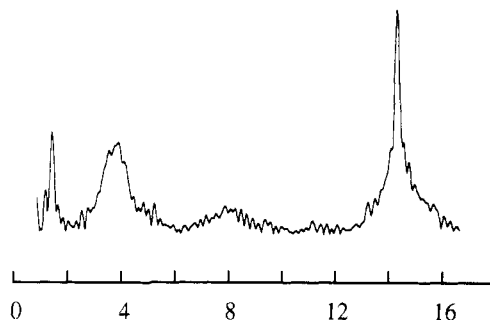


Figure 4. Three-pulse ESEEM spectrum of a Mn²⁺-GDP p21 complex containing ¹⁵N amide labeled glycine (73%). The spectrum was obtained at a field setting of 3364 G, EPR frequency of 9.867 GHz, and fixed delay between the first two pulses of 344 ns. Peaks are apparent at the ¹⁵N and ¹H Larmor frequencies (1.5 and 14.3 MHz). The ³¹P Larmor peak is absent, and the ³¹P _{β} fundamentals at ~ 4 MHz and ~ 8 MHz are distorted, owing to suppression effects and spectrometer dead time (ref 7b,c).

spectra. Detailed simulation, with accounting for isotopic enrichment as assessed by GC/MS, yields $A_2^0 = -0.15 \pm 0.03$ MHz and a value of 3.8 ± 0.3 Å for the distance between the Mn²⁺ and the serine 17 amide nitrogen. This distance is slightly less than the 4.5-Å distance found by crystallography.

For the glycine amide labeled protein featured in the upper traces of Figures 2 and 3, the X-ray crystal structure suggests that the majority of the ¹⁵N modulation should arise from glycines 13 and 60, with smaller contributions from glycines 12 and 15. Although we cannot separate the contributions of each glycine to the ESEEM, spectral simulation based on the crystallographic distances is entirely consistent with the observed amplitude. The amplitude of ¹⁵N Larmor frequency peak exhibited in the three-pulse ESEEM spectrum shown in Figure 4 enables us to establish a lower bound distance for a single glycine ¹⁵N of 5.4 Å. Analysis of the ESEEM at the ³¹P Larmor frequency establishes that $A_2^0 = 0.21 \pm 0.03$ MHz from which we calculate the distance from the Mn²⁺ to the α -phosphorus of the GDP to be 5.3 ± 0.1 Å, in good agreement with the crystallographic distance of 5.5 Å.

Conclusions

Our results demonstrate the utility of ESEEM spectroscopy in the determination of structural details of proteins in non-crystalline media, when selective isotopic labels can be introduced and the degree of isotopic enrichment can be assayed. The high multiplicity of the Mn²⁺ electron spin system introduces no serious difficulties in the quantitative interpretation of the p21 ESEEM spectra. We have determined hyperfine coupling constants for several nuclei and from them have determined interatomic distances that are in excellent agreement with those obtained by X-ray crystallography. This close agreement suggests that Mn²⁺ substitution does not significantly alter the protein structure. Our results indicate that this method will be useful for probing an individual spin $1/2$ nucleus within ~ 6 Å from the Mn²⁺ probe; this field-of-vision can be extended by the use of ²H labels and multiple labeling (e.g., -CD₃ methyl labeling).^{23,24} Finally, we note that with ~ 0.5 mM samples the sensitivity in these experiments is excellent, with single-acquisition signal-to-noise ratios of $\sim 40:1$ for echoes obtained at an interpulse of ~ 250 ns. Inasmuch as GAP-p21 complexes are soluble at millimolar concentrations,²⁵ these results suggest that ESEEM will play a fruitful role in the study of interactions between GAP and p21 proteins.

(17) Dikanov, S. A.; Astashkin, A. V. *Advanced EPR: Applications in Biology and Biochemistry*; Hoff, A. J., Ed.; Elsevier: Amsterdam, 1989; pp 59–118.

(18) (a) LoBrutto, R.; Smithers, G. S.; Reed, G. H.; Orme-Johnson, W. H.; Tan, S. L.; Leigh, J. S. *Biochemistry* **1986**, *25*, 5654–5660. (b) Eads, C. D.; LoBrutto, R.; Kumar, A.; Villafranca, J. J. *Biochemistry* **1988**, *27*, 165–170. (c) Tipton, P. A.; McCracken, J.; Cornelius, J. B.; Peisach, J. *Biochemistry* **1989**, *28*, 5720–5728.

(19) (a) Larsen, R. G.; Halkides, C. J.; Papastavros, M. Z.; Redfield, A. G.; Singel, D. J. *Frontiers in NMR on Molecular Biology-II*, Keystone, CO, April 1991. (b) Larsen, R. G.; Halkides, C. J.; Redfield, A. G.; Singel, D. J. 14th International EPR Symposium; 33rd Rocky Mountain Conference on Analytical Chemistry, Denver, CO, July 1991. (c) Larsen, R. G.; Halkides, C. J.; Singel, D. J. *J. Chem. Phys.* Submitted for publication.

(20) Lai, A.; Flanagan, H. L.; Singel, D. J. *J. Chem. Phys.* **1988**, *89*, 7161–7166.

(21) The sign assignment of M_s is based on the measured relative sign of A_0^0 and A_2^0 and on the assumption that the sign for A_2^0 is that of the classical dipole interaction, consistent with the convention used in ref 20.

(22) Atomic coordinates of the structure described in ref 4b were obtained from I. Schlichting and E. F. Pai.

(23) (a) Mims, W. B.; Davis, J. L.; Peisach, J. *J. Magn. Reson.* **1990**, *86*, 273–292. (b) Kevan, L. *Time Domain Electron Spin Resonance*; Kevan, L., Schwartz, R. N., Eds.; Wiley: New York, 1979; pp 279–341.

(24) (a) Yudanov, Y. F.; Salikhov, K. M.; Zhidomirov, G. M. *Zh. Strukt. Khim.* **1969**, *10*, 732. (b) Yudanov, Y. F.; Salikhov, K. M.; Zhidomirov, G. M. *J. Struct. Chem.* **1969**, *10*, 625.

(25) Halkides, C.; Redfield, A. G. Unpublished results.

Acknowledgment. This work is supported in part by NIH Grant CA51992 to Frank McCormick of Chiron Corp., who also supplied us with the N-ras plasmids; NIH Training Grants GM08313 and GM07598 (RGL); and an NIH postdoctoral fellowship, CA 08872 (C.J.H.). We are grateful to Emil Pai and Ilme Schlichting for access to unpublished atomic coordinates of p21, to Mary Pastavros for technical assistance in the preparation of the protein samples, to Rebecca Meyers for assistance with the GC/MS analysis, and to Steve Branch for helpful discussions about the GC/MS procedures. We also thank George Reed for originally suggesting ESEEM experiments on p21.

Appendix: Comments on Mn²⁺ ESEEM

In the Mn²⁺·GDP complexes of p21, the $S = 5/2$ multilevel electron spin system is adequately regarded as comprised of noninteracting, resonant two-level systems with constituent levels characterized by the quantum number M_s . The ESEEM response of a nucleus coupled to Mn²⁺ can be described as a sum of the responses associated with each two-level system, weighted by its contribution to the spin-echo. The weights vary with the position of microwave excitation within the EPR powder pattern. The weights are readily calculated in a manner analogous to that which we introduced for the determination of orientational selectivity factors.^{14,26,27}

For nuclear spin $I = 1/2$ systems, the two-pulse ESEEM response from each two-level system may be written as:

$$E(\tau) = 1 - (k/4)[2 - 2 \cos(2\pi\nu_\kappa\tau) - 2 \cos(2\pi\nu_\lambda\tau) + \cos(2\pi(\nu_\kappa - \nu_\lambda)\tau) + \cos(2\pi(\nu_\kappa + \nu_\lambda)\tau)] \quad (1)$$

in which:

$$k = \left[\frac{3\nu_n A_2^0 \cos \theta (M_s^\kappa - M_s^\lambda)}{\nu_\kappa \nu_\lambda} \right]^2 \quad (2)$$

and ν_κ or ν_λ are given by:

$$\nu_{\kappa,\lambda} = [(\nu_n + M_s^{\kappa,\lambda} A_0^0 + M_s^{\kappa,\lambda} A_2^0 (1 - 3 \cos^2 \theta))^2 + (3M_s^{\kappa,\lambda} A_2^0 \sin \theta \cos \theta)^2]^{1/2} \quad (3)$$

In eqs 1 - 3, τ is the time between microwave pulses, ν_n is the nuclear Larmor frequency, ν_κ and ν_λ are the nuclear frequencies in the κ and λ electron spin levels, A_0^0 is the isotropic hyperfine coupling constant, A_2^0 is the anisotropic hyperfine coupling constant, and θ is the angle between the external field and the major axis of the hyperfine interaction.

As detailed in previous work,²⁰ the modulation depth parameter, k , attains its maximum value when, in either the κ or λ spin level, the hyperfine and Zeeman interactions are equal in magnitude and opposed in sign, or "matched". This match occurs within a limited range of nuclear Zeeman frequencies bounded by $|M_s(A_0^0 + 2A_2^0)|$ and $|M_s(A_0^0 - A_2^0)|$. A line-narrowing of the fundamental ESEEM peaks occurs in this same ν_n range. This effect is readily recognized by rewriting expression 3 as:

$$\nu_{\kappa,\lambda} = [(\nu_n + M_s^{\kappa,\lambda}(A_0^0 - A_2^0))^2 + 3M_s^{\kappa,\lambda} A_2^0 \cos^2 \theta (2\nu_n + M_s^{\kappa,\lambda}(2A_0^0 + A_2^0))]^{1/2} \quad (4)$$

from which it is seen that the dispersion caused by the anisotropy of the hyperfine interaction is suppressed, that is, the final term of eq 4 is cancelled, when $\nu_n = |M_s(2A_0^0 + A_2^0)|/2$ and the Zeeman and hyperfine interactions are of opposite sign. The matching of the Zeeman and hyperfine interactions, with attendant amplitude resonance and line-narrowing effects, are primary factors in determining the appearance ESEEM spectra.^{19,20} In systems of high electron spin multiplicity, a sequence of matching and line-narrowing situations occurs associated with the succession of allowed values of $|M_s|$.

(26) Gerfen, G. J.; Singel, D. J. *J. Chem. Phys.*, submitted for publication.
(27) Cosgrove, S. A. Applications of Electron Spin Echo Envelope Modulation Spectroscopy to Catalytic Systems. Ph.D. Thesis, Harvard University, 1992.

EXAFS Evidence for a "Cysteine Switch" in the Activation of Prostromelysin

Richard C. Holz,[†] Scott P. Salowe,[§] Catherine K. Smith,^{§,†} Gregory C. Cuca,[§] and Lawrence Que, Jr.*[‡]

Contribution from the Department of Chemistry, University of Minnesota, Minneapolis, Minnesota 55455, and the Department of Biophysical Chemistry, Merck Research Laboratories, Rahway, New Jersey 07065. Received April 20, 1992

Abstract: Zn K-edge EXAFS data of the matrix metalloproteinase (MMP) stromelysin-1 were obtained in both its latent proenzyme and mature active forms. The Fourier-filtered (back-transform 0.7–2.3 Å) χk^3 spectrum of mature stromelysin was satisfactorily simulated with 4 N/O scatterers per Zn at 2.01 Å, while similar fits for prostromelysin were judged unacceptable because of unreasonable Debye–Waller factors or significantly larger residuals of the fits. For prostromelysin, excellent fits were obtained with the introduction of a sulfur scatterer at 2.25 Å. These data provide the first direct evidence for the coordination of zinc by the sole cysteine in the N-terminal domain of prostromelysin and confirm that the cysteine is lost upon activation. These results provide support for a "cysteine switch" structural model for MMP proenzymes that suggests the interaction of the conserved propeptide cysteine with zinc is present in the latent form. Examination of the Zn–S bond length and outer shell carbon contributions suggests that the 2 g-atoms of zinc recently shown to be present in stromelysin (Salowe, S. P., et al. *Biochemistry* 1992, 31, 4535–4540) reside in independent zinc sites.

Introduction

Stromelysin-1 is a metalloendoproteinase which is able to degrade a broad range of extracellular components in connective tissue matrices and may be a central agent in the proteolytic

destruction of cartilage proteoglycans associated with osteo- and rheumatoid arthritis. Stromelysin is one member of the matrix metalloproteinase (MMP) family of enzymes which are characterized by their high primary sequence similarity, requirement for Ca²⁺ and Zn²⁺, and secretion as inactive proenzymes.¹ It was recently demonstrated that the N-terminal catalytic domain of stromelysin-1, in fact, contains two zinc sites, with one site clearly

[†]University of Minnesota.

[§]Merck Research Laboratories.

[‡]Present address: Department of Molecular Biophysics & Biochemistry, Yale University, New Haven, CT.

(1) Woessner, J. F. *FASEB J.* 1991, 5, 2145–2154.